Heliyon 9 (2023) e18318

Contents lists available at ScienceDirect

Heliyon

journal homepage: www.cell.com/heliyon

Microfluidics-based PLGA nanoparticles of ratiometric multidrug: From encapsulation and release rates to cytotoxicity in human lens epithelial cells

Yexuan Guo [a], Xinyang Li [b], Robert B. Macgregor Jr. [c], Hong Yan [a,b,**], Rui Xue Zhang [a,*]

[a] *Xi'an Key Laboratory of Stem Cell and Regenerative Medicine, Institute of Medical Research, Northwestern Polytechnical University, 127 West Youyi Road, Xi'an, Shaanxi 710072, China*

[b] *Xi'an People's Hospital (Xi'an Fourth Hospital), Shaanxi Eye Hospital, Affiliated People's Hospital of Northwest University, 21 Jiefang Road, Xi'an, Shaanxi 710004, China*

[c] *Department of Pharmaceutical Sciences, Leslie Dan Faculty of Pharmacy, University of Toronto, 144 College Street, Toronto, Ontario M5S 3M2, Canada*

ARTICLE INFO

Keywords:
PLGA
Release mechanism
Bioavailability
Microfluidics
DoE
Combination therapy
Posterior capsule opacification

ABSTRACT

Multidrug nanomedicine is an effective therapeutic approach for the treatment of chronic diseases and cancers. However, co-encapsulation and release of drug combination at a fixed ratio by nanoparticles, particularly for long acting ocular formulations, remains challenging. Herein, poly (lactic-co-glycolic acid) nanoparticles ratiometrically co-encapsulating hydrophilic dual drugs, mitomycin C and doxorubicin, was obtained (D/M PLGANPs) by combining microfluidics and the Design of Experiments approaches. The formulation variable of lactide-to-glycolide ratios (L/G 50:50, 75:15 and 85:15) was used to achieve fast, medium and slow drug release rates of D/M PLGANPs. The dissolution of D/M PLGANPs in simulated intraocular fluid exhibited sustained release of dual drugs at the fixed ratio over 7 days, and analysis using the *Korsmeyer-Peppas* model showed mechanism of drug release to be governed by diffusion. More importantly, in human lens epithelial cells, the drug release rate was negatively correlated with drug potency. The slower drug release from D/M PLGANPs led to lower efficacy of drug combination against pathogenesis of cellular migration and proliferation, the key pathogenic processes of capsular opacification after cataract surgery. Compared to fast (L/G 50:50) and medium (L/G 75:15) drug release rate of D/M PLGANPs, the slow release formulation (L/G 85:15) exhibited the least cellular uptake of the dual drugs and the ratio of drug combination was not maintained intracellularly. The present study implicates the potential of using microfluidics for synthesizing polymeric nanoparticles of ratiometric drug combination and highlights the drug release rate as the critical determinant of efficacy for the long-acting nanomedicine design.

* Corresponding author.

** Corresponding author. Xi'an Key Laboratory of Stem Cell and Regenerative Medicine, Institute of Medical Research, Northwestern Polytechnical University, 127 West Youyi Road, Xi'an, Shaanxi 710072, China.

E-mail addresses: yan2128ts@med.nwu.edu.cn (H. Yan), zhangruixue@nwpu.edu.cn (R.X. Zhang).

https://doi.org/10.1016/j.heliyon.2023.e18318
Received 29 June 2023; Received in revised form 13 July 2023; Accepted 13 July 2023
Available online 15 July 2023

1. Introduction

Nanomedicines that co-encapsulate multiple drugs are increasingly recognized as useful medications for managing cancers and chronic diseases [1,2]. Examples of nanomedicine that have demonstrated ratiometric co-encapsulation of drug combination include liposomes, such as CPX-351, the antineoplastic liposomal drugs combination (cytarabine and daunorubicin) at the fixed ratio, polymer-based nanocarrier, micelles (e.g., Triolimus) and polymer-lipid hybrid nanoparticles [3–9]. Compared to other dosage forms (e.g., microparticles, hydrogel), multidrug nanomedicines can undergo cellular uptake as a unit cargo to enable subcellular drug delivery at a fixed ratio, thereby producing synergistic therapeutic efficacy. To date, nanocarriers have been used mostly for anticancer therapy in which the drug release was only a few days [10,11]. For long-acting formulations used for chronic diseases, the implementation of nanomedicine remains challenging due to the demand of dosing multiple drugs over a sustained period of time (e.g., >1 week).

Posterior capsular opacification (PCO), for example, is a chronic, multifactorial eye disease as a consequence of post-cataract surgical wound healing response where viable lens epithelial cells (LECs) undergo aberrant repopulation, migration and fibrosis in the capsular bag [12]. To prevent PCO, combination of select chemotherapeutic drugs that target a collection of those pathological processes in LECs are thought to be effective [12–14]. For instance, doxorubicin (DOX) and mitomycin C (MMC) are potent cytotoxic drugs, which have been administered intraoperatively as single agents at high doses (e.g., milligram) to ablate LECs. However, free in solution, these two drugs are prone to rapid elimination from the aqueous humor and can cause unwanted ocular toxicity to surrounding tissues [15–17]. In human LECs as well as cancer cells, the fixed-dose MMC and DOX combination (MMC-DOX) can synergistically reduce cell viability at markedly lower concentrations than single agent treatment [18,19], which suggests that co-delivery of MMC-DOX may lead to favorable outcomes in the effort to control the pathogenesis of LECs. Unlike anticancer therapy, which is administered intravenously at specific intervals, prevention of PCO involves intraoperative single-dosing of the pharmacological agent (s) [20,21]. Thus, a long-acting formulation capable of ratiometric drug release is highly preferable in PCO drug therapy.

The biodegradable co-polymer poly (lactic-co-glycolic) acid (PLGA) has been extensively exploited because of its biodegradability and controlled drug release [22,23]. In particular, PLGA is available with different molecular weights (M_W), end-caps (i.e., ester and acid), copolymer composition (i.e., lactide-to-glycolide (L/G) ratios), and non-linear types (e.g., star-shape) [24]. With these diverse properties, PLGA can be employed to create tailored drug release profiles for drug delivery systems [24]. In clinic, two PLGA ocular implants, Ozurdex and Durysta, have been available for sustained release drug delivery of dexamethasone and bimatoprost, respectively, for up to 3–6 months [25,26]. In preclinical studies, PLGA-based nanoparticles (PLGANPs) loaded with a single drug improved corneal residence time and intraocular penetration of drugs [27–29]. However, so far, there are few literature reports on the delivery of drug combinations by PLGANPs for PCO prevention; this is due, in part to the general difficulty of coordinating the kinetics of multidrug release by nanoparticles.

In the present study, a series of PLGANPs co-encapsulating small, hydrophilic DOX and MMC (D/M PLGANPs) at a molar ratio of 1:3 were synthesized *via* microfluidics using PLGA polymers with M_W around 80 kDa and L/G ratios of 50:50, 75:25 and 85:15 (Fig. 1A). To

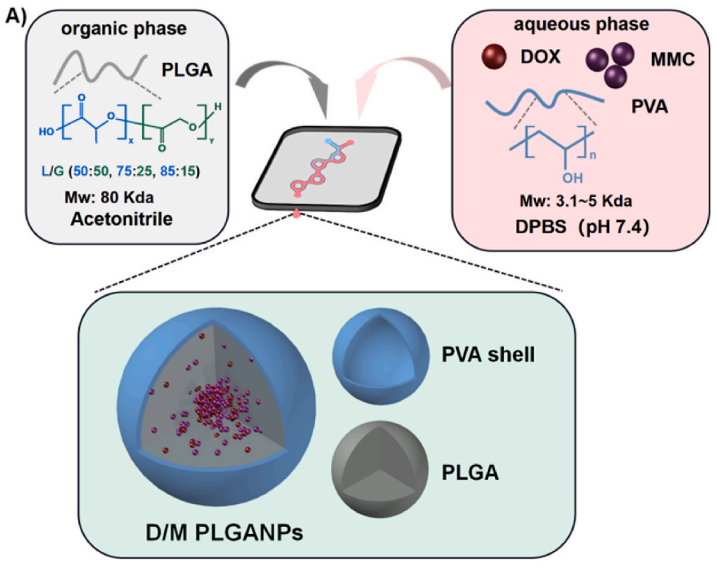

B)

L/G	FRR (flow rate ratio) (aqueous:organic)	TFR (total flow rates) (mL/min)
50:50	1:1	5
	1:1	15
	3:1	10
	5:1	5
	5:1	15
75:25	1:1	10
	3:1	5
	3:1	10
	3:1	10
	3:1	10
	3:1	15
	5:1	10
85:15	1:1	5
	1:1	15
	3:1	10
	5:1	5
	5:1	15

Fig. 1. Synthesis of D/M-PLGANPs using an integrated microfluidics and the DoE approach. A) Illustration of *in situ* formation of the PLGANPs ratiometrically co-loaded with DOX-MMC on a staggered herringbone micromixer using microfluidics. The grey box (left) represents organic phase of PLGA polymers with 80 kDa M_W but different L/G ratios dissolved in acetonitrile. In the structure of PLGA, x and y denote the number of lactide (L) and glycolide (G) units, respectively. The pink box (right) represents aqueous phase of hydrophilic drugs (i.e., DOX and MMC) at a fixed molar ratio of 1:3 and stabilizer PVA with 3.1–5 kDa M_W dissolved in DPBS (pH 7.4); B) DoE based microfluidic flow settings (FRR and TFR) used for the assembly of D/M PLGANPs with three L/G ratios, 50:50, 75:25 and 85:15.

obtain ratiometrically drug co-loaded D/M PLGANPs, the Design of Experiment (DoE) approach was applied to investigate the effect of microfluidic flows (i.e., aqueous and organic phases) on *in situ* formation of PLGANPs of drug combination. Nano-structural crystallinity and compositional interactions (e.g., drug-particles) of D/M PLGANPs were also examined to confirm co-encapsulation of MMC-DOX by nanoparticles. D/M PLGANPs of varied L/G ratios exhibited sustained release of MMC and DOX at the fixed synergistic ratio over one week. We also studied the effect of the L/G ratio on the release rate of the drugs from PLGANPs by monitoring the viability, uptake, and migration of human LECs.

2. Materials and methods

2.1. Materials

DOX hydrochloride (98.47% purity), MMC (99.47% purity) and thiazolyl blue tetrazolium bromide (99.84%) were purchased from MedChemExpress LLC (Shanghai, China). PLGA ester terminated (L/G ratio 75:25, M_W 76–115 kDa), poly (vinyl alcohol) (PVA) (v 31–50 kDa, 87–89% hydrolyzed) and dimethyl sulfoxide (DMSO) were bought from Sigma-Aldrich LLC (Shanghai, China). PLGA ester terminated (L/G ratios: 50:50, M_W 80 kDa; L/G ratio:85:15, M_W 80 kDa) were obtained from Xi'an RuixiBiotech Co., Ltd (Shaanxi, China). HPLC-graded acetonitrile was purchased from Ourchem® Co., Ltd (Shanghai, China). Compound electrolyte intraocular irrigating solution (Shike®) was purchased from SINQI (Liaoning, China). Ultrapure water (H_2O) was obtained from Milli-Q Synergy with UV Water Purification System, USA. Sterile Dulbecco's phosphate buffered saline (DPBS) and 1 × Hank's balanced salt solution (1 × HBSS) were purchased from HAT (Shaanxi, China). Fetal bovine serum (FBS) was purchased from Shuangru Biotech (Shanghai, China). Minimum essential medium (MEM) and penicillin-streptomycin solution (100 ×) were bought from Hyclone, USA.

2.2. Microfluidic synthesis of PLGANPs

D/M PLGANPs with various L/G ratios of 50:50, 70:25, 85:15 were synthesized using microfluidics with the NanoAssemblr® Ignite instrument (Precision Nanosystems Inc., Canada). In brief, the aqueous phase was prepared by dissolving PVA (0.5% w/v), DOX (0.2 mM) and MMC (0.6 mM) in DPBS and the organic phase was prepared by dissolving PLGA (1% w/v) in acetonitrile. PLGANPs were self-assembled by mixing appropriate volumes of PLGA solution with aqueous phases on a staggered herringbone chaotic structured microfluidic cartridge (Precision Nanosystems Inc., Canada). The microchannel had 0.5 mm in diameter and was made of cycloolefin polymer. The microfluidic flow parameters were set at various total flow rates (TFR) between 5 and 15 mL/min and at an aqueous to organic flow rate ratio (FRR) between 1:1 and 5:1 v/v. The PLGANPs without loaded drugs (Blank-PLGANPs) as controls were prepared in the same way except drugs were not added to the aqueous solution. PLGANPs were dialyzed against 2 L of DPBS at room temperature for 1 h at a stirring speed of 100 rpm using a dialysis membrane with 300 kDa molecular weight cut-off (MWCO) (Solarbio, Beijing, China). Proton nuclear magnetic resonance (1H-NMR) analysis was performed to confirm the removal of residual organic solvent acetonitrile (Supplementary Materials (Suppl. Mater.) S1). The purified PLGANPs were stored at 4 °C for further studies.

2.3. DoE approach to D/M PLGANPs optimization

A DoE with 3 factors and 3 levels (MODDE®, Sartorius, Germany) was used to select desirable properties of D/M PLGANPs, in which the factors included were L/G ratios, FRR and TFR corresponding to the values (low, medium, and high) of 50:50, 75:25 and 85:15 for L/G ratios, 1:1, 3:1 and 5:1 (v/v) for FRR and 5, 10 and 15 mL/min for TFR, respectively (Fig. 1B). The parameter responses, including the hydrodynamic size, polydispersity index (PDI), drug encapsulation efficiency of DOX and MMC (EE-DOX% and EE-MMC %) of D/M-PLGANPs, were determined. The data collected in each experimental run was analyzed by multiple linear regression (MLR) to estimate the coefficients of the Central Composite Face (CCF) design prediction model. Analysis of variance (ANOVA) was performed to validate the model based on R^2, Q^2, model validity and reproducibility as the goodness of fit and prediction (Suppl. Mater. S2). The final D/M-PLGANPs satisfied the following characteristics: 100 nm $<$ size $<$250 nm, PDI $<$0.2; maximum and similar values for both EE-DOX% and EE-MMC% to maintain the fixed ratio of MMC-DOX. Specifically, D/M PLGANPs with varied L/G ratios, denoted as D/M PLGANPs-50, D/M PLGANPs-75 and D/M PLGANPs-85, were obtained by setting TFR and FRR at 15 mL/min and 5:1 v/v, 5 mL/min and 2.3:1 v/v and 10 mL/min and 3:1 v/v, respectively, according to the DoE prediction model.

2.4. Physicochemical characterization of D/M-PLGANPs

Before formulation characterization, PLGANPs were filtered using 0.44 μm polyethersulfone membrane filter. A ten-fold diluted PLGANPs suspension in ultra-pure H2O was used to determine the size, PDI, and ξ-potential using the NanoBrook 90Plus PALS instrument (Brookhaven Instrument, USA). To determine EE% and drug loading capacity (LC%) of DM-PLGANPs, freshly prepared 6 mL of DM-PLGANPs was ultra-centrifuged at 200,000×g, 4 °C for 30 min (BECKMAN COULTER, Optima XPN-100, USA), and the supernatant containing unencapsulated MMC and DOX was collected and assayed at 360 nm and 480 nm, respectively by the multifunction microplate reader (Tecan-Tecan Spark™, Switzerland). To visualize the particle size and shape, D/M PLGANPs were diluted at a concentration of 0.1 mg/mL and further coated with gold by an ion sputter module (MC1000, Hitachi) on a crystalline silicon wafer (BZS0505, China Electron Microscopy Network). The images of D/M-PLGANPs were acquired using the ultrahigh resolution field emission scanning electron microscopy (FESEM) (VeriosG4, FEI-Thermo Fisher Scientific). The detailed sample preparation of SEM was described in Suppl. Mater. S3. For the stability study, D/M PLGANPs were incubated in compound electrolyte

intraocular irrigating solution at 1:1 (v/v) at 37 °C over 7d. At the predetermined time points, the size and PDI of PLGANPs were measured.

2.5. Structural and compositional analysis of D/M PLGANPs

Powder X-ray diffraction patterns (PXRD) of free drugs (i.e., DOX and MMC), various PLGANPs and physical mixture of PLGANPs and free drugs were recorded at room temperature with a diffractometer (D8 A25 DISCOVER, Bruker, Germany). Lyophilized samples were loaded onto a glass sample holder and scanned using Co Kα radiation at a voltage of 40 kV and 30 mA. The data were collected between 5° and 90° 2θ in a continuous scan with a scan angular speed of 2°/min.

Compositional interactions of D/M PLGANPs were also analyzed by an attenuated total reflectance Fourier-transform infrared spectroscopy (ATR-FTIR) (Nicolet iS 50, Thermo, USA), and the wavenumber ranged from 500 cm^{-1} to 4000 cm^{-1}. The particle sample was concentrated using an ultrafiltration centrifuge tube (UFC5003BK, MerckMillipore) at 14000 ×g and 4 °C for 30 min, and then dropped onto a diamond ATR unit. DPBS as the aqueous background was subtracted from each spectrum. All the spectra were processed by OriginPro (OriginLab, Northampton, USA).

2.6. In vitro drug release of D/M PLGANPs

Dual drug release kinetics of D/M PLGANPs with different L/G ratios, including D/M PLGANPs-50, D/M PLGANPs-75 and D/M PLGANPs-80, were determined using a dialysis method. In brief, one mL of D/M PLGANPs were encased in a dialysis tube with a MWCO 300 kDa, and then incubated in 10 mL of compound electrolyte intraocular irrigating solution (pH 7.4) at 37 °C and a stirring speed of 100 rpm, avoiding the light. At pre-determined timepoints (0.25h, 0.5h, 1h, 3h, 6h, 9h, 12h, 1d, 2d, 3d, 4d, 5d, 6d, 7d), 100 μL of dissolution medium outside the dialysis bag was withdrawn followed by replenishing an equal volume of pre-warmed fresh buffer. DOX and MMC concentrations were quantitated spectrophotometrically at 480 nm and 360 nm, respectively. Free DOX-MMC at the molar ratio of 1:3 was used as the control. The drug-release profiles of DOX and MMC from D/M PLGANPs were fitted by DDSolver using the Korsmeyer-Peppas model with an add-in program for Microsoft Excel previously developed by Zhang et al., from China Pharmaceutical University [30]. The goodness of fit among models was evaluated based on the statistical criteria of adjusted coefficient of determination (R2adjusted), mean square error (MSE), standard deviation of the residuals (MSE), Akaike information criterion (AIC), and model selection criterion (MSC) (Suppl. Mater. S4).

2.7. Cellular drug uptake and localization of D/M PLGANPs

The human lens epithelial cell line HLE-B3 (BNCC, China) was maintained in the MEM supplemented with 10% FBS and 0.5% (v/v) penicillin-streptomycin at 37 °C in a humidified incubator with 5% CO_2 atmosphere (Suppl. Mater. S5). Cells were seeded on a round coverslip (Biosharp, China) in a 24-well plate at a density of 2.5×10^4 per well and allowed to grow for 12 h. Before treatment, cells were starved in the serum-free medium for additional 2 h. Cells were then incubated with various D/M PLGANPs for 40 min at the DOX concentration of 8 μM. To visualize the intracellular localization of DOX, following the incubation, HLE-B3 cells were washed three times with DPBS and the nuclei were labeled with the fluorescent dye 4′,6-diamidino-2-phenylindole (DAPI) (GeneCopoeia, China) at a concentration of 5 μg/mL for 10 min at 37 °C. The DAPI staining solution was aspirated, and cells were rinsed three times with pre-warmed DPBS. The cells on the round coverslip were loaded onto a slide and imaged using a confocal laser scanning microscope (CLSM) (FV3000, Olympus, Japan). Cells were imaged at 405 nm (blue channel) and 561 nm (red channel) laser light to visualize nuclei (blue) and DOX (red), respectively. To quantitate cellular drug uptake, after 40 min exposure to the treatment, the medium was removed, and cells were washed three times with DPBS. The amount of DOX and MMC was measured at 480 nm and 360 nm by the multi-function microplate reader, respectively.

2.8. Transwell migration assay

The cell migration ability was assessed using a 24-well Matrigel chamber (8.0-μm pore size, polycarbonate membrane) (LABSELECT, China). Firstly, HLE-B3 cells suspended in 100 μL of XX were plated at the density of 1×10^4 per well in the upper wells of the Transwell plates. Various PLGANPs, including blank and drug loaded particles, were added to the upper wells at the DOX concentration of 8 μM, while 600 μL of MEM complete medium containing 5 ng/mL of TGF-β2 was added to the bottom chamber. The cells were incubated at 37 °C for 24 h and 48 h. Then, the non-migratory cells were removed from the upper side of chamber membrane with cotton swabs. To quantify the migrating cells, cells on the lower surface of the membrane were fixed with 4% paraformaldehyde (HAT, China) at room temperature for 30 min, and then stained with 0.1% crystal violet (Beyotime, China) for 30 min at room temperature. The number of migratory cells per chamber was counted by the ImageJ (version 1.51j8, USA) with the threshold and size set at (0.85) and 65 pixel, respectively.

2.9. Cytotoxicity against HLE B-3 cells

HLE B-3 cells were plated at the density of 1 × 104 cells per well in a 96-well plate overnight before any treatment. Cells were then treated by Blank PLGANPs and D/M PLGANPs with different L/G ratios at various concentration from 0.25 to 128 μM for 3 h or 24 h. All the treatment concentrations were based on the concentration of DOX loaded into D/M PLGANPs. Before conducting MTT ((3-[4,5-

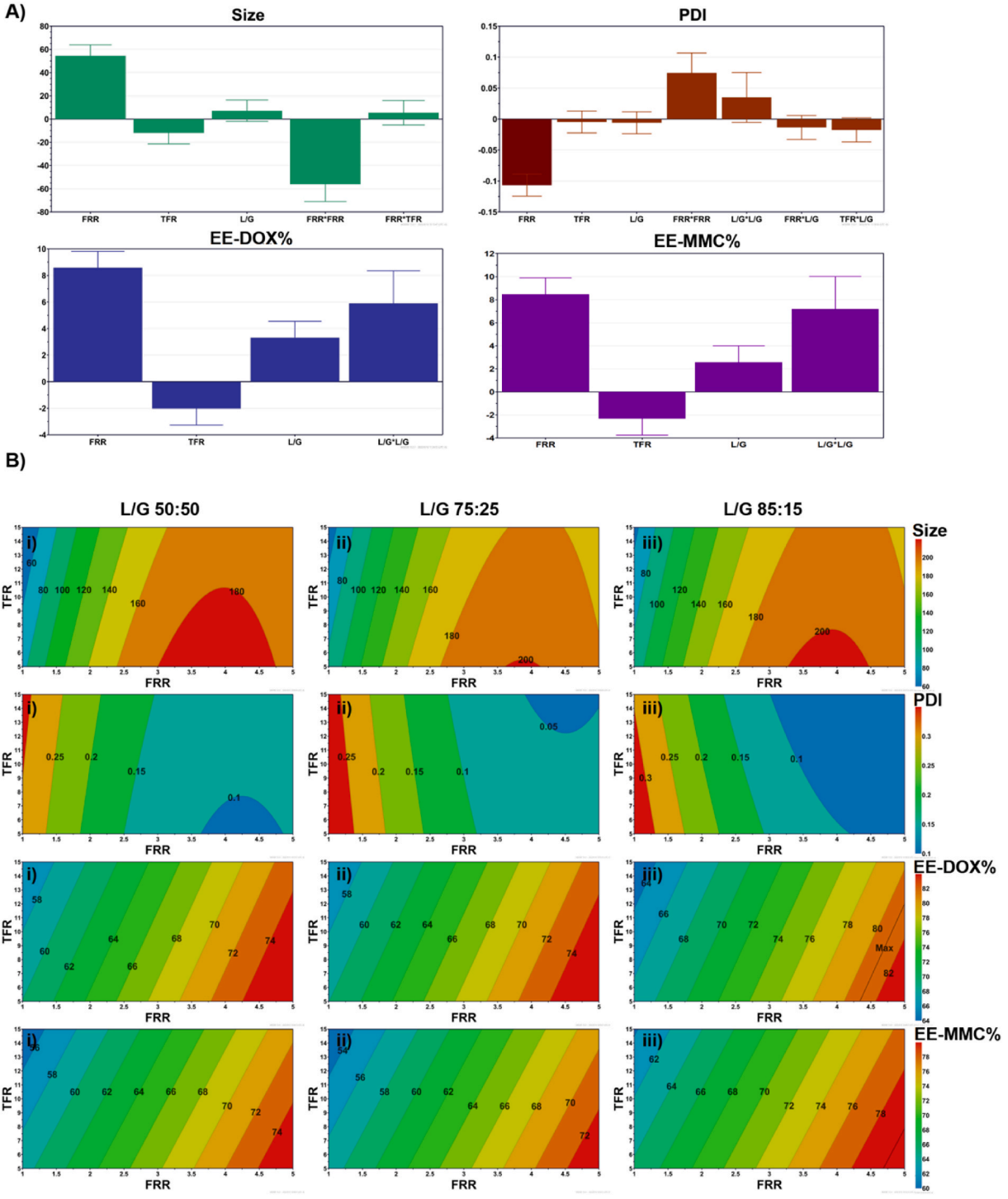

Fig. 2. MLR analysis of DoE prediction model for microfluidics parameters. A) Plots of coefficient terms in CCF model for size, PDI, EE-DOX% and EE-MMC% of D/M PLGANPs analyzed by MLR fit method. Coefficient terms determined as statistically significant with $p < 0.05$ were presented in the plot; B) Two-dimensional contour maps showing effects of varying FRR, TFR and L/G ratios on physicochemical characteristics of D/M PLGANPs, from the top to bottom, nanoparticle size, size distribution (i.e., PDI), drug entrapment of EE%-DOX, and drug entrapment of EE%-MMC. Note, the color gradient from blue to red indicates the parameter values from low to high. Specific values are shown within each contour.

A)

L/G	FRR	TFR (mL/min)
50:50	5.0:1	15
75:25	2.3:1	5
85:15	3.0:1	10

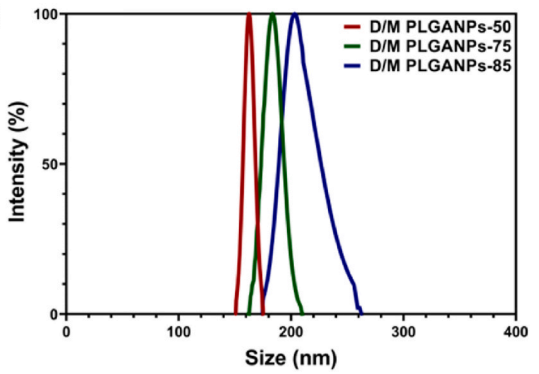

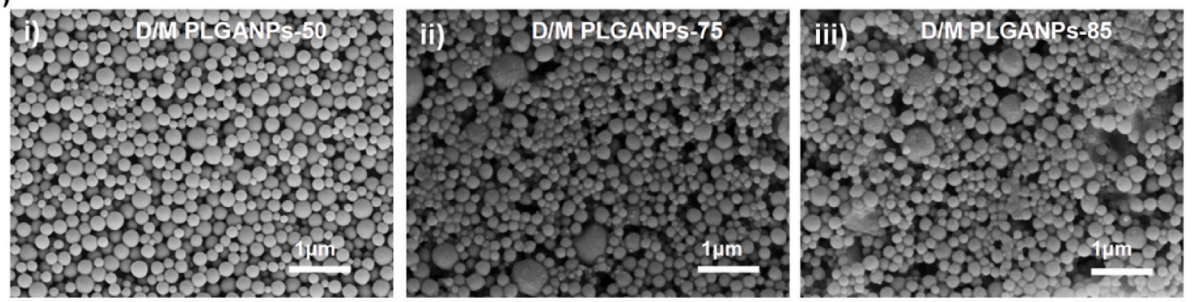

D)

Emulsions	Size (nm)	PDI	ξ-potential (mV)	EE-DOX%[a]	LC-DOX%[b]	EE-MMC%[a]	LC-MMC%[b]	MMC:DOX (molar ratio)
D/M PLGANPs-50	160.32±10.38	0.06±0.02	-5.31±2.62	73.15±5.64	1.97	71.56±8.54	3.59	2.93±0.35
D/M PLGANPs-75	183.24±12.63	0.08±0.01	-7.49±3.19	65.69±6.09	0.86	62.71±9.29	1.78	2.86±0.42
D/M PLGANPs-85	201.46±11.37	0.12±0.01	-9.41±4.12	73.23±4.36	1.30	70.54±7.25	2.33	2.89±0.29

[a] Encapsulation Efficiency(EE%) = (1-free drug amount /total added drug) x 100%
[b] Loading Capacity(LC%) = amount of encapsulated drug/total mass of PLGANPs x 100%

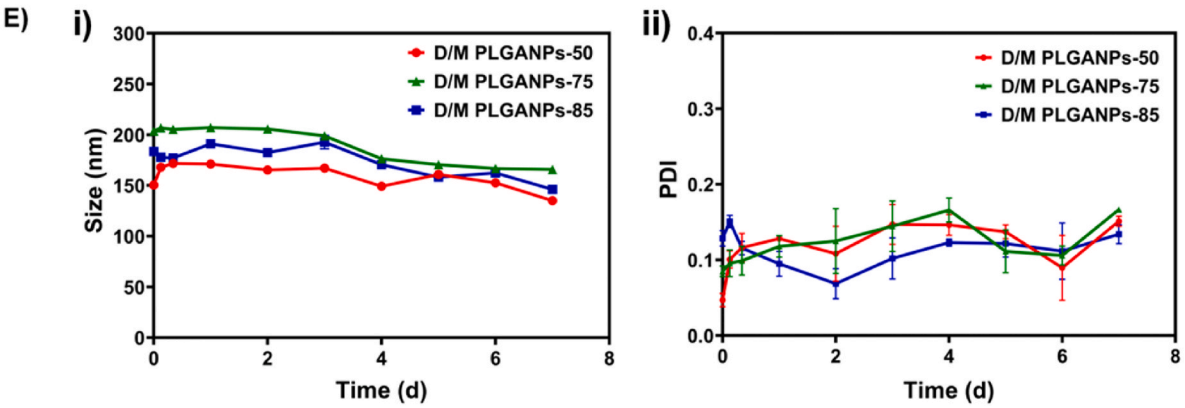

Fig. 3. Physicochemical characterization of three D/M PLGANPs with L/G ratios of 50:50, 75:25 or 85:15. A) Select microfluidic flow settings (FRR and TFR) of D/M PLGANPs preparation based on the DoE prediction model; B) Representation of the particle size distribution; C) SEM nanoscale images for morphological analysis of particles; D) Particle sizes, PDI, ζ-potential, drugs EE% and LC%; E) Nanoparticle stability in compound electrolyte intraocular irrigating solution at 37 °C for 7 d as measured in i) size and ii) PDI. Data are presented as mean ± SEM (n = 3). The SEM bar in Fig. 3E i) was too small to be visible, and it was less than 5 nm.

dimethylthiazol-2-yl]-2,5-diphenyl tetrazolium bromide) assay, the treatment medium was removed from each well, and cells were washed once with DPBS. MTT cell viability assay was performed according to the manufactural instruction (Suppl. Mater. S8). The concentration of formazan was analyzed at 490 nm with the multi-function microplate reader.

2.10. Statistical analysis

All data were analyzed using GraphPad Prism (version 9.02, USA) and presented as mean ± standard error of mean (SEM). For *in vitro* cellular uptake and migration studies, statistical significance among PLGANPs groups and within the same formulation was analyzed by two-way ANOVA followed by *Dunnett's* multiple comparison test among groups and non-paired Student's *t*-test, respectively. The statistically significant difference was defined as *$p < 0.05$, **$p < 0.01$, ***$p < 0.001$ and ****$p < 0.0001$.

3. Results

3.1. Effects of microfluidic parameters on physicochemical properties of D/M PLGANPs

We first screened microfluidic parameters of TFR and FRR as well as L/G ratios at 3-levels using DoE approach followed by DoE-based CCF model analysis for the goodness-of-fit (Suppl. Mater. S2). Fig. 2 shows MLR analysis of each factor and their interactions (i.e., TFR, FRR and L/G ratios) as well as their two-dimensional contour maps of predictive results of CCF model to visualize the effects of TFR and FRR on size, PDI, EE-DOX% and EE-MMC% of D/M PLGANPs using different L/G ratios in PLGANPs. Firstly, the data in Fig. 2 show that an increase of FRR level from 1:1 to 1:5 v/v prominently affected all measured properties of D/M PLGANPs, including increased particle size, the EE% of the drugs, and decreased PDI. Compared to FRR, the effect of TFR had negative correlation and less impact on the size, PDI, and the EE% of the drugs for the D/M PLGANPs; that is, EE-DOX% and EE-MMC% decreased with the increase of TFR. Moreover, the increase of L/G ratio levels from 50:50 to 85:15 affected the values of measured responses in varied extent. The particle size and drug entrapment (e.g., EE-DOX% and EE-MMC%) of D/M PLGANPs exhibited positive correlations, whereas PDI had negative correlation with L/G ratios; that is, the increase in L/G ratios led to the increased size and EE% but decreased PDI. Because the summary statistics of DoE-based CCF model was not significant for ζ-potential (Suppl. Mater. Table 1S), the two-dimensional contour

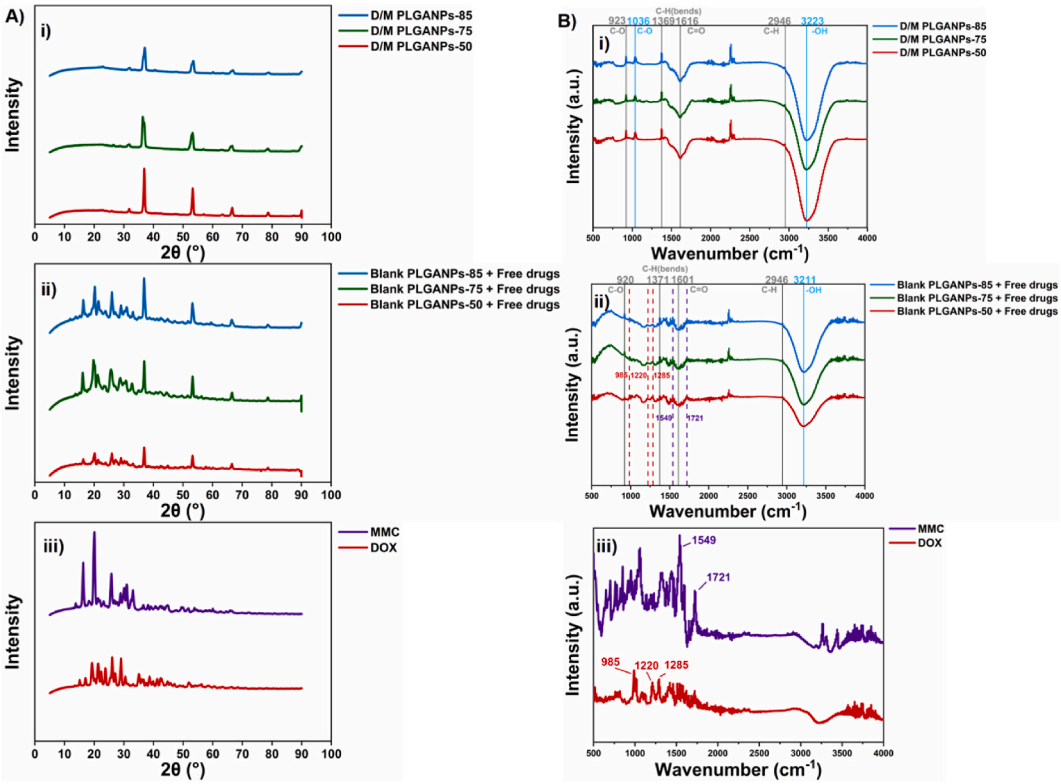

Fig. 4. Crystallinity and drug-particle interactions of three D/M PLGANPs with L/G ratios of 50:50, 75:25 or 85:15. A) XRD patterns of i) D/M PLGANPs, ii) physical mixture of Blank PLGANPs and free drugs (DOX and MMC) and iii) free drugs (DOX and MMC); B) ATR-FTIR spectrum of i) D/M PLGANPs, ii) physical mixture of Blank PLGANPs and free drugs and iii) Free DOX-MMC. The vertical dotted lines of red and purple are the characteristic peaks of DOX and MMC, respectively. The grey and blue vertical lines represent the characteristic peaks of PLGA and PVA, respectively.

map was not plotted. The specific quantification of the specific change trend in the two-dimensional Contour line map is shown as the coefficient terms in Fig. 2 A). It is possible to visually observe the quantification degree of specific response results by different factors and their interactions, that is, by giving a preset condition, the predicted value of a specific response result can be calculated from the graph.

3.2. D/M PLGANPs exhibited similar physiochemical properties and ratiometric drug payloads

D/M PLGANPs with three different L/G ratios, denoted by D/M PLGA-50, D/M PLGA-75 and D/M PLGA-85, were synthesized by setting-up the value ranges of measured responses (i.e., particle size, minimum PDI, and maximum drugs EE%) using the DoE predictive model. The specific synthesis parameters for D/M PLGA-50, D/M PLGA-75 and D/M PLGA-85 are shown in Fig. 3A. As shown in Fig. 3B, C and D, all D/M PLGANPs using selected microfluidics parameters were within targeted range of values of physiochemical properties: 100 nm < size <250 nm, PDI <0.2; maximum and similar values for both EE-DOX% and EE-MMC% to maintain the fixed ratio of MMC-DOX. The maximum drug loading capacity for DOX and MMC (DOX-LC% and MMC-LC%) of D/M PLGANPs were 1.97% and 3.59%, respectively. Specifically, D/M PLGANPs had narrow particle size distribution with PDI between 0.06 and 0.12 and particle size diameters between 160 nm and 200 nm. The values of the ζ-potential of D/M PLGA were negative and ranged from −5 to −8 mV. Consistent with dynamic light scattering measurements, SEM micrographs showed a nanosized, spherical morphology of all D/M PLGANPs, and some larger NPs in D/M PLGANPs-85. The increase of L/G ratios from 50:50 to 85:15 in D/M PLGANPs resulted in the formation of larger size of PLNGANPs as can be seen in Fig. 3C. More importantly, the drug entrapment of both MMC-DOX within the three D/M PLGANPs reached more than 65% and achieved ratiometric co-encapsulation at 3:1, the ratio of MMC-DOX initially dissolved in the aqueous phase. In compound electrolyte intraocular irrigating solution at 37 °C, all three D/M PLGANPs maintained good stability as evidenced by the minor changes in particle sizes and PDI observed over 7 days. The colloidal stability and ratiometric co-encapsulation of D/M PLGANPs provided a basis for subsequent drug release studies.

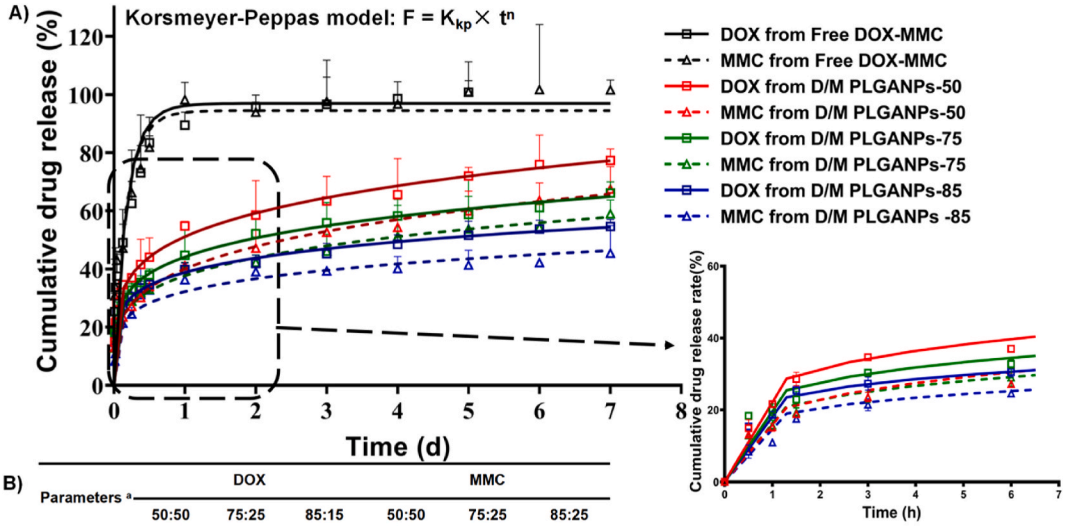

B)

Parameters [a]	DOX			MMC		
	50:50	75:25	85:15	50:50	75:25	85:25
K_{kp}	51.059	44.095	38.768	39.948	37.629	32.157
n	0.212	0.198	0.173	0.255	0.218	0.187
T_{50} (d)	0.905	1.949	4.406	2.46	4.454	10.888
T_{80} (d)	8.393	20.623	68.977	16.564	58.839	141.269
AUC	444.057	377.335	322.598	365.220	330.227	271.733
MRT(d)	2.893	3.114	3.247	3.054	3.178	3.300
MDT(d)	1.247	1.180	1.060	1.443	1.288	1.127

C)

Emulsions	MMC:DOX (AUC ratio)
D/M PLGANPs-50	2.46
D/M PLGANPs-75	2.63
D/M PLGANPs-85	2.53

[a] K_{Kp} : the release constant incorporating structural and geometric characteristics of the dosage form;
n: the diffusional exponent indicating drug release mechanisms, T_{50} and T_{80} :the time for 50% and 80% of drug to appear in solution; AUC: the area under the drug release curve ; MRT: mean residence time of the drug molecules in the dosage form; MDT: mean dissolution time.

Fig. 5. Sustained ratiometric drug release kinetics of DOX and MMC from three D/M PLGANPs suspensions with L/G ratios of 50:50, 75:25 or 85:15 in compound electrolyte intraocular irrigating solution. A) Fitted cumulative drug release profiles of DOX and MMC from D/M PLGANPs; B) Characteristic parameters of drug release curves from various D/M PLGANPs. The drug release data was fitted according the *Korsmeyer-Peppas* model using the DDSolver software program. The geometric shape of PLGANPs was spherical; C) AUC ratio of MMC and DOX released over 7 days. The drug release kinetics was performed in compound electrolyte intraocular irrigating solution at 37 °C for 7 days using the dialysis method. Free DOX-MMC at the same combined ratio and concentration was used as the control. Data were presented as mean ± SEM (n = 3–5). The MW of PLGA was between 76 and 115 kDa.

3.3. Crystallinity of loaded drugs and their interactions with PLGANPs

To gain insight into the interactions of co-encapsulated MMC-DOX with PLGANPs, their crystallinity and functional groups were studied using PXRD and FTIR, respectively (Fig. 4). Compared to the diffraction patterns of blank PLGANPs (Fig. S2 in Suppl. Mater. S4), free MMC-DOX, physical mixture of Blank PLGANPs + Free drugs was characterized of prominent diffractogram at 2θ of 15°–30° and 35°–55°, respectively (Fig. 4A). In contrast, for D/M PLGANPs, no diffraction pattern of drugs was observed at diffraction angles (2θ) between 15° and 30°, indicating that complete drug encapsulation in the polymeric PLGANPs leaving the diffractograms with only the polymer diffraction patterns.

The drug-PLGANPs interactions were studied using ATR-FTIR. As shown in Fig. 4B, free MMC-DOX showed peaks at 985 cm^{-1} (N–H peak), 1220 cm^{-1} and 1285 cm^{-1} (C–C and C–O vibrations peaks) which are characteristic for DOX and at 1549 cm^{-1} (amide II peak) and 1721 cm^{-1} (amide I peak) for MMC, respectively. In the blank PLGANPs (Fig. S2 in Suppl. Mater. S4), the characteristic peaks of PLGA [31] included 920 cm^{-1} (C–O peak), 1371 cm^{-1} (-CH2), 1608 cm^{-1} (C=O peak) and 2946 cm^{-1} (C–H peak), and of PVA [32] included 1036 cm^{-1} (C–O–C peak) and 3223 cm^{-1}(O–H peak). In the physical mixtures of Blank PLGANPs + Free drugs, the characteristic peaks of MMC-DOX and PLGA were seen without position alterations; however, the characteristic peaks of PVA at 1036 cm^{-1} was masked and 3223 cm^{-1} was shifted to 3211 cm^{-1}, respectively. For D/M PLGANPs, the characteristic peaks of MMC-DOX were masked by the peaks in the spectrum of PLGA and PVA. Compared to blank PLGANPs, corresponding bands of PLGA were shifted from 920 cm^{-1} to 923 cm^{-1} for C–O stretch, from 1371 cm^{-1} to 1369 cm^{-1} for C–H bends, and from 1608 cm^{-1} to 1616 cm^{-1} for C=O stretch [33,34]. In addition, the peak intensity of PVA was increased in D/M PLGA compared to the physical mixture and blank PLGANPs. These results indicate that MMC-DOX was present within the core of PLGANPs.

3.4. Sustained ratiometric drug release of D/M PLGANPs

The drug release profiles of MMC-DOX from various D/M PLGANPs were determined using dialysis. All of D/M PLGANPs exhibited biphasic release curves and continuously released drugs for 7 days with more than 20% of initial burst release of both drugs within 3 h and more than 50% drugs released by the 7th day (Fig. 5A). Moreover, increasing the L/G ratios from 50:50 to 85:15 led to a decrease in the drug release rate of D/M PLGANPs. Using the DDSolver software, the drug-release data of MMC-DOX were fitted best to *Korsmeyer-Peppas* model, the goodness of fit indicated by statistical criteria (**Suppl. Mater. S5**). Fig. 5B shows the characteristic parameters of DOX and MMC release curves of each D/M PLGANPs obtained by the fit to the *Korsmeyer-Peppas* model. With the increase

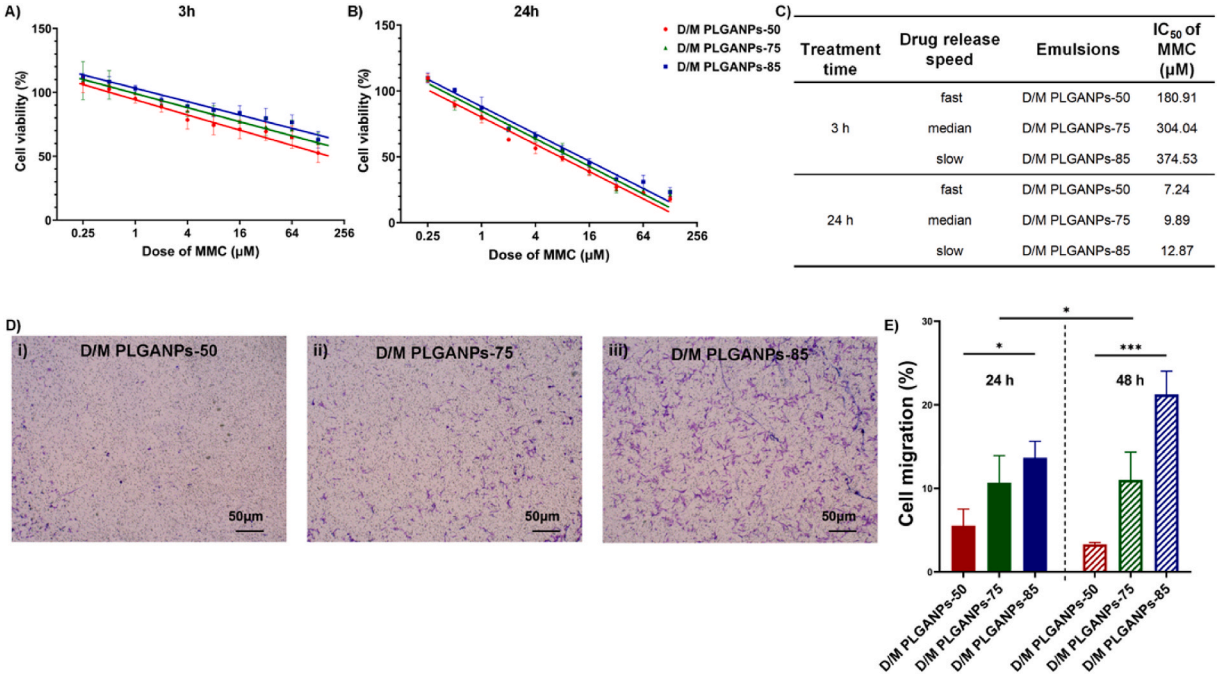

Treatment time	Drug release speed	Emulsions	IC_{50} of MMC (μM)
3 h	fast	D/M PLGANPs-50	180.91
	median	D/M PLGANPs-75	304.04
	slow	D/M PLGANPs-85	374.53
24 h	fast	D/M PLGANPs-50	7.24
	median	D/M PLGANPs-75	9.89
	slow	D/M PLGANPs-85	12.87

Fig. 6. Drug release rate dependent efficacy of D/M PLGANPs with fast, median and slow drug release in the human HLE-B3 cells. A) and B) Percent cell viability (%) of HLE-B3 after exposure to D/M PLGANPs suspensions for 3 h and 24 h, respectively. X-axis showed the dose of MMC only; C) IC_{50} of MMC after 3 h and 24 h exposure to various D/M PLGANPs; D) Photographs (magnification, 200x) of crystal violet stained cells at 48 h. Note that MMC concentration was based on the molar ratio of drug entrapment in each D/M PLGANPs; E) Transwell migration assay determining the cell migration percent (%) at 24 h and 48 h. Cells were stimulated by 5 ng/mL TGF-β2 while treated with D/M PLGANPs at DOX concentration of 8 μM. Data were presented as mean ± SEM (n = 3) with *$p < 0.05$ and ***$p < 0.001$. Cell viability was assessed by the MTT assay. Corresponding dose of DOX was at DOX-MMC molar ratio of 1:3. Data were presented as mean ± SEM (n = 3–5).

of L/G ratios in PLGANPs, the release velocity constant (K_{kp}) decreased 1.32 fold, the time required for releasing the equivalent amounts of drugs was prolonged up to 8.52 fold (as evidenced by the values of T_{50}, T_{80}, and MRT of the drugs within PLGANPs), and mean dissolution time (MDT) of both drugs (MMC-DOX). D/M PLGANPs had the exponent of release (*n*) relating to the drug release mechanisms smaller than 0.43, suggesting the release of MMC-DOX from PLGANPs was governed by Fickian diffusion [35]. In addition, the value of *n* decreased with the increase of L/G ratios, indicating that the increase of L/G ratio led to the greater effect of diffusion on the drug release mechanism of D/M PLGANPs. More importantly, D/M PLGANPs released dual drugs at nearly the same release rate as evidenced by similar ratios of AUC (area under the curve) of cumulative release percent of MMC and DOX around 2.5:1 (Fig. 5C), which were within the range of the synergistic ratio of MMC-DOX and close to the drug co-encapsulation ratios of 2.9:1.

3.5. Drug release rate dependent efficacy of D/M PLGANPs

LEC proliferation and migration to the posterior capsule of the eye is one of major pathological activities post cataract surgery, eventually leading to PCO formation. For this reason, the cytotoxicity and anti-migration effects of the long-acting D/M PLGANPs with different drug release rates were evaluated in human LEC. In Fig. 6, human HLE-B3 cells were exposed to D/M PLGANPs with the fast, median, and slow release, namely D/M PLGANPs-50, D/M PLGANPs-75 and D/M PLGANPs-85. As shown in Fig. 6A–C, IC_{50} of D/M PLGANPs with fast release was up to 2-fold higher than slow release one, indicating the altered potency of drug combination using different drug release carrier. Moreover, as the exposure time increased from 3 h to 24 h, the cell viability curves became steeper, which demonstrates the dependence of the cytotoxicity on the dose and exposure time of D/M PLGANPs. The doses for 50% of cell viability inhibition (IC_{50}) over 24 h exposure time were up to 31-fold lower than 3 h.

We further measured the migratory response of LEC using the Transwell migration assay by co-incubating HLE-B3 cells with the stimulating cytokine TGF-β2 and PLGANPs for 24 h and 48 h. As shown in Fig. 6D&E **(Suppl. Mater. S7.)**

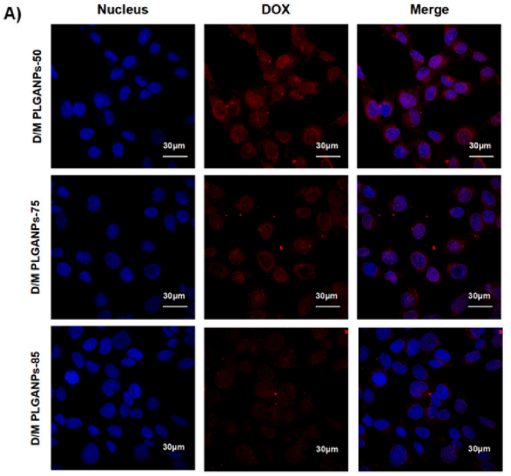

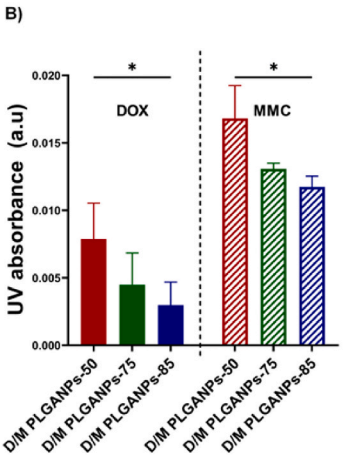

C)

Emulsions	Drug release speed	MMC:DOX (UV absorbance ratio)
D/M PLGANPs-50	fast	2.14
D/M PLGANPs-75	median	2.91
D/M PLGANPs-85	slow	3.94

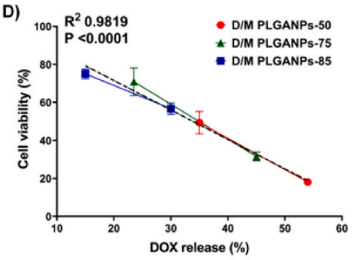

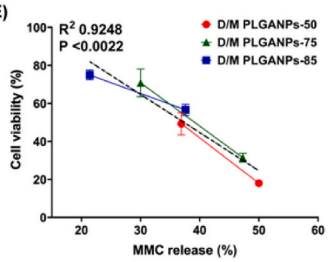

Fig. 7. Effects of drug release rate on cellular uptake and potency of D/M PLGANPs. A) CLSM images (60 × objective lens) of DOX intracellular location. From left to right, first panel, nuclei (blue); second panel, DOX (red); third panel, DOX/Hoechst merged; B) & C) UV quantification of cellular drugs accumulation of D/M PLGANPs. DOX and MMC uptake were measured at 480 nm and 360 nm, respectively, with the UV–vis spectrophotometer. Cells were incubated with D/M PLGANPs for 40 min at DOX concentration of 8 μM; D) & E) Correlation of released DOX and MMC doses and cell viability (%). The data were replotted using the data from Fig. 5A, for DOX and MMC release from various D/M PLGANPs at 3 h and 24 h corresponding to cell viability (%). There was a strong inverse correlation between drug release (%) and cell viability (%), $R^2 > 0.90$ ($p < 0.05$).

3.6. Underlying mechanism of differential efficacy of D/M PLGANPs

To investigate underlying mechanism attributing to differential cytotoxicity and antimigration effect of D/M PLGANPs, the cellular drug uptake of D/M PLGANPs were evaluated in human LEC. Intracellular distributions of DOX after 40 min treatment with D/M PLGANPs were imaged using CLSM (Fig. 7A). The red fluorescent signal of drug DOX within cells decreased as the L/G ratios of PLGANPs increased from 50:50 to 85:15. The fast release D/M PLGANPs-50 resulted in DOX localization in both nucleus and cytoplasm whereas the slow release D/M PLGANPs-85 led to sparse, discrete, red dots distributed in the cytoplasm. Quantitative analysis of cellular drugs accumulation in HLE-B3 cells showed significant difference among three D/M PLGANPs suspensions as evidenced by the absorbance reduction of both DOX and MMC with increased L/G ratios (Fig. 7B). The UV absorbance ratios of MMC-DOX of three D/M PLGANPs were 2.14, 2.91 and 3.94, respectively (Fig. 7C), implying varied concentration ratios of drug combination upon cellular uptake. It is worth noting that the median release D/M PLGANPs-75 exhibited the nearest drug-to-drug ratios (i.e., 2.91:1) to the ratio of the initial drug entrapment (i.e., 2.86:1), whereas the slow release D/M PLGANPs-85 did not maintain the fixed synergistic ratio (i.e., 3.94:1).

To further analyze whether drug release rates of three D/M PLGANPs would be a contributing factor, the relationship between cell viability (%) and drug release (%) (i.e., DOX and MMC) of three D/M PLGANPs obtained from Fig. 5 were re-plotted (Fig. 7D&E). The different color data sets (red, green and blue) represent the percent drug release corresponding to the percent cell viability at 3 h and 24 h. It clear from the data that exposure to DM PLGANPs led to a decrease in cell viability; the correlation coefficients being $R^2 = 0.9819$ ($p < 0.0001$) for DOX and $R^2 = 0.9248$ ($p < 0.0022$) for MMC. These results suggest that the potency of drug combination was affected by their rate of drug release of PLGANPs.

4. Discussion

The present study, we describe the microfluidics-based synthesis of PLGANPs co-encapsulating hydrophilic dual drugs, MMC-DOX, at the fixed ratio of 3:1. Encapsulation of small, hydrophilic drug(s) into a PLGA-structured network by conventional technique of bulk-mixing-nanoprecipitation (e.g., double suspension) has been challenging, due to slow mixing and rapid partitioning of the drug into the dispersing water phase before the formation of PLGANPs [36–38]. Nanoprecipitation assisted by the use of microfluidics involves the fast and tunable mixing of aqueous and organic solutions that contains drug(s) and hydrophobic PLGA polymer; this method has been extensively applied to PLGANPs drug delivery systems [39,40]. In the present work, we combined microfluidics and DoE for tuning the mixing process (i.e., TFR and FRR) to optimize the co-encapsulation MMC-DOX into PLGANPs using various L/G ratio (i.e., 50:50, 75:25, and 85:15) (Fig. 1). Our findings are consistent with those of a study in which a similar approach was applied for loading a small hydrophilic drug (i.e., N-acetylcysteine) into PLGANPs, FRR had more effect than TFR on the size, polydispersity and the EE% of the drug [41]. By concomitantly adjusting TFR and FRR, D/M PLGANPs with MMC and DOX encapsulation >65%, sizes <250 nm, and PDI values less than 0.2 were obtained for different L/G ratios of PLGA (Fig. 2). Because MMC and DOX are hydrophilic and have low M.W. (334 and 580 Daltons, respectively), we observed similar time scales for precipitation of both drugs into PLGANPs using microfluidics under the same TFR and FRR [42]. Accordingly, MMC-DOX at a molar ratio of 3:1 in aqueous PBS can be ratiometrically co-entrapped into PLGANPs by tuning the solvent mixing (i.e., TFR and PBS to acetonitrile ratio) (Fig. 3). The positive correlation between L/G ratios in PLGA and drug EE% may attribute to an increase in the interaction or affinity of both drugs to with the lactide moiety as evidenced by FTIR spectrum in which the C=O and C–H bands of PLGANP were markedly shifted after drug encapsulation (Fig. 4), indicating most drugs were encapsulated within the PLGANPs core. Studies using other methods, such as O/W single suspension and sonication, also found that amount of lactide of PLGA increased the entrapment efficiency of drugs, although the drug entrapment yield of PLGANPs was relatively low, around 20% compared to 65% of microfluidics [43,44].

The drug release mechanisms of PLGA-based drug delivery systems are complex, including the polymer hydrolysis and erosion, water adsorption and swelling, and drug diffusion, among which drug transport through water-filled pores driven by diffusion is the most common way of drug release [24]. Similarly, the diffusion process enabled precise ratiometric control over MMC-DOX release from D/M PLGANPs, and its drug release behavior was well described by the *Korsmeyer-Peppas* model with the high goodness of fit (Fig. 5). The *Korsmeyer-Peppas* model remains one of the most popular in modeling PLGA drug release, and the diffusional exponent n for spherical PLGANPs was 0.43 or less implicating mechanism of Fickian diffusion [35,45,46]. This was further evidenced by reduced *n* from 0.255 to 0.173 as the L/G ratio of D/M PLGANPs increased from 50:50 to 85:15, suggesting the drug release was more dominated by diffusion than PLGA hydrolysis (Fig. 5B&C).

In the present study, D/M PLGANPs of three different L/G ratios had similar size and drug content, and their drug release rate was controlled by the L/G ratio of PLGANPs; that is, the increase in L/G ratio (e.g., from 50:50 to 85:15) resulted in more hydrophobic PLGANPs matrix that is less degraded by water penetration. Incorporation of low L/G ratio (e.g.,50:50) in PLGANPs may be speculated to increase the rate of drug release by facilitating diffusion through loosely packed hydrophilic water pocket in PLGANPs. The phenomenon of initial burst drug release of all PLGANPs suspension was observed by our and other research groups using various preparation methods [47–49]. Although D/M PLGANPs was purified, the water-influx into PLGANPs triggered the drug release close to the PLGANPs surface. As demonstrated in Fig. 5A inset, PLGANPs had the initial fast drug release within the first few hours, for which its profile followed the diffusion driven mechanism. It is worth noting that the dialysis for D/M PLGANPs purification may lead to minor drug loss due to drugs “locked out” before PLGANPs formation and adsorbed at the particle surface upon exposure to the dialysis fluid (i.e., DPBS) [50].

Drug release rate is a critical factor to determine the therapeutic efficacy of the drug delivery system. In LEC, D/M PLGANPs with different drug release rates showed different therapeutic effects. In theory, after cataract surgery, to eliminate residual LEC, D/M

PLGA-50 and D/M PLGA-75 with rapid and medium release was potent against LEC growth whereas the slow release D/M PLGA-85 was inadequate due to the lack of therapeutic drug concentration in the short period of time (i.e., 48 h). On one hand, the long-acting ocular formulation with sustained drug release is the desirable to reduce repeated drug injection [51,52]. Increase in L/G ratio from 50:50 to 85:15 markedly prolongs the degradation of PLGA from 1 month to up to 6 months, resulting in continuous drug delivery [53]. On the other hand, drug release rates that are too slow result in poor drug bioavailability, which in turn reduces the drug effectiveness. As demonstrated in human LEC treated by D/M PLGANPs with fast, medium and slow release rates, the slow release D/M PLGA had the least uptake into the cell nucleus where the action of drugs occurs and the fixed ratio of MMC-DOX was not maintained at the cellular level. The low potency of D/M PLGA-85 with the slow release rate on LEC migration and proliferation, the key pathogenetic processes of PCO formation, was a further indication of the low drug concentration of the drugs (Figs. 6 and 7). Thus, the balance between sustained drug release and drug release rate is important for designing long-acting PLGANPs for PCO therapies.

5. Conclusion

In conclusion, PLGANPs were developed to ratiometrically co-encapsulate and release the drug combination MMC-DOX (D/M PLGANP) using the combined microfluidics and the DoE approach. D/M PLGANPs inhibited pathological activities of human LECs responsible for PCO formation such as migration and growth. Spherical D/M PLGANPs exhibited good colloidal stability and sustained release of the two drugs in intraocular irritating solution. The release mechanism of both MMC and DOX from D/M PLGANPs analyzed by the *Korsmeyer-Peppas* fitted model was dominated by diffusion. More importantly, alteration of L/G ratio in PLGANPs formulation significantly affected release rates of MMC-DOX, which in turn, influenced cellular drug uptake and efficacy of D/M PLGANPs in human LECs. The present study sheds light on the critical role of drug release kinetics in designing efficacious nanomedicines and underscores the potential utility of PLGANPs for multidrug delivery for long-acting treatment of PCO.

Funding

This work is supported by Key Research and Development Projects of Shaanxi Province (2021ZDLSF02-08), High-end Foreign Experts Recruitment Plan of China (G2022183018L), National Natural Science Foundation of China (81873674, 82070947 and 81570823), the Innovative Capability Support Program of Shaanxi (2023-CX-TD-72) and Xi'an Talent Program (XAYC200021).

Author contribution statement

Y. Guo performed the experiments and wrote the paper; X. Li analyzed and interpreted the data; R.B. Macgregor Jr contributed wrote the paper and analyzed and interpreted the data; H. Yan contributed reagents, materials, analysis tools or data; R.X. Zhang conceived and designed the experiments and wrote the paper.

Data availability statement

Data will be made available on request.

Declaration of competing interest

The authors declare that they have no known competing financial interests or personal relationships that could have appeared to influence the work reported in this paper.

Acknowledgements

Authors greatly appreciate the following individuals and facilities: Weijia Lu and Jing Su (graduate students, Northwestern Polytechnical University) for mathematical analysis of synergistic drug combination and DoE predication model, respectively; Dr. Ganlan Bian (Institute of Medical Research, Northwestern Polytechnical University) for CLSM image acquisition; Analytical & Testing Center (Northwestern Polytechnical University) for FESEM and PXRD analysis of nanoparticles; Institute of Flexible Electronics (Northwestern Polytechnical University) for 1H-NMR analysis of PLGANPs.

Abbreviations

Blank-PLGANPs non-drug loading PLGANPs
D/M PLGANPs PLGANPs co-encapsulating doxorubicin and mitomycin C
DoE design of experiment
DOX doxorubicin
EE% drug encapsulation efficiency
Free DOX-MMC combined doxorubicin and mitomycin C in solution
FRR flow rate ratio
LECs lens epithelial cells

L/G ratio lactide-to-glycolide ratio
MMC mitomycin C
PDI polydispersity index
PLGANPs poly(lactic-co-glycolic acid) nanoparticles
PLGA poly(lactic-co-glycolic acid)
PVA poly(vinyl alcohol)
TFR total flow rate

Appendix A. Supplementary data

Supplementary data to this article can be found online at https://doi.org/10.1016/j.heliyon.2023.e18318.

References

[1] A.M. Sofias, T. Lammers, Multidrug nanomedicine, Nat. Nanotechnol. 18 (2023) 104–106, https://doi.org/10.1038/s41565-022-01265-3.
[2] R.X. Zhang, H.L. Wong, H.Y. Xue, et al., Nanomedicine of synergistic drug combinations for cancer therapy - strategies and perspectives, J. Contr. Release 240 (2016) 489–503, https://doi.org/10.1016/j.jconrel.2016.06.012, 2016/06/12.
[3] J.E. Lancet, G.L. Uy, J.E. Cortes, et al., CPX-351 (cytarabine and daunorubicin) liposome for injection versus conventional cytarabine plus daunorubicin in older patients with newly diagnosed secondary acute myeloid leukemia, J. Clin. Oncol. 36 (2018) 2684–2692, https://doi.org/10.1200/jco.2017.77.6112, 20180719.
[4] A. Detappe, H.V. Nguyen, Y. Jiang, et al., Molecular bottlebrush prodrugs as mono- and triplex combination therapies for multiple myeloma, Nat. Nanotechnol. 18 (2023) 184–192, https://doi.org/10.1038/s41565-022-01310-1, 20230126.
[5] S. Aryal, C.-M.J. Hu, L. Zhang, Polymeric nanoparticles with precise ratiometric control over drug loading for combination therapy, Mol. Pharm. 8 (2011) 1401–1407, https://doi.org/10.1021/mp200243k.
[6] T. Lammers, V. Subr, K. Ulbrich, et al., Simultaneous delivery of doxorubicin and gemcitabine to tumors in vivo using prototypic polymeric drug carriers, Biomaterials 30 (2009) 3466–3475, https://doi.org/10.1016/j.biomaterials.2009.02.040, 20090321.
[7] J.R. Hasenstein, H.C. Shin, K. Kasmerchak, et al., Antitumor activity of Triolimus: a novel multidrug-loaded micelle containing Paclitaxel, Rapamycin, and 17-AAG, Mol. Cancer Therapeut. 11 (2012) 2233–2242.
[8] R.X. Zhang, P. Cai, T. Zhang, et al., Polymer–lipid hybrid nanoparticles synchronize pharmacokinetics of co-encapsulated doxorubicin–mitomycin C and enable their spatiotemporal co-delivery and local bioavailability in breast tumor, Nanomed. Nanotechnol. Biol. Med. 12 (2016) 1279–1290, https://doi.org/10.1016/j.nano.2015.12.383.
[9] J. Su, W. Lu, Y. Guo, et al., Depot unilamellar liposomes to sustain transscleral drug Co-delivery for ophthalmic infection therapy, J. Drug Deliv. Sci. Technol. 86 (2023), 104629, https://doi.org/10.1016/j.jddst.2023.104629.
[10] R.X. Zhang, J. Li, T. Zhang, et al., Importance of integrating nanotechnology with pharmacology and physiology for innovative drug delivery and therapy – an illustration with firsthand examples, Acta Pharmacol. Sin. 39 (2018) 825–844, https://doi.org/10.1038/aps.2018.33.
[11] R.X. Zhang, T. Ahmed, L.Y. Li, et al., Design of nanocarriers for nanoscale drug delivery to enhance cancer treatment using hybrid polymer and lipid building blocks, Nanoscale 9 (2017) 1334–1355, https://doi.org/10.1039/c6nr08486a, 2016/12/16.
[12] I.M. Wormstone, Y.M. Wormstone, A.J.O. Smith, et al., Posterior capsule opacification: what's in the bag? Prog. Retin. Eye Res. 82 (2021), 100905 https://doi.org/10.1016/j.preteyeres.2020.100905.
[13] L.M. Nibourg, E. Gelens, R. Kuijer, et al., Prevention of posterior capsular opacification, Exp. Eye Res. 136 (2015) 100–115, https://doi.org/10.1016/j.exer.2015.03.011.
[14] G.A. Peyman, K. Hosseini, Combination therapies in ophthalmology: implications for intravitreal delivery, J. Ophthalmic Vis. Res. 6 (2011) 36–46.
[15] R. Guha, S. Chowdhury, H. Palui, et al., Doxorubicin-loaded MePEG-PCL nanoparticles for prevention of posterior capsular opacification, Nanomedicine 8 (2013) 1415–1428, https://doi.org/10.2217/nnm.12.175.
[16] C.M. Haus, A.L. Galand, Mitomycin against posterior capsular opacification: an experimental study in rabbits, Br. J. Ophthalmol. 80 (1996) 1087, https://doi.org/10.1136/bjo.80.12.1087.
[17] R.J. Derick, L. Pasquale, H.A. Quigley, et al., Potential toxicity of mitomycin C, Arch. Ophthalmol. 109 (1991) 1635, https://doi.org/10.1001/archopht.1991.01080120013002.
[18] A.J. Shuhendler, P.J. O'Brien, A.M. Rauth, et al., On the synergistic effect of doxorubicin and mitomycin C against breast cancer cells, Drug Metabol. Drug Interact. 22 (2007) 201–233, https://doi.org/10.1515/dmdi.2007.22.4.201, 2008/05/02.
[19] A.J. Shuhendler, P. Prasad, R.X. Zhang, et al., Synergistic nanoparticulate drug combination overcomes multidrug resistance, increases efficacy, and reduces cardiotoxicity in a nonimmunocompromised breast tumor model, Mol. Pharm. 11 (2014) 2659–2674, https://doi.org/10.1021/mp500093c.
[20] Ü.Ü. İnan, F. Öztürk, S. Kaynak, et al., Prevention of posterior capsule opacification by intraoperative single-dose pharmacologic agents, J. Cataract Refract. Surg. 27 (2001) 1079–1087, https://doi.org/10.1016/S0886-3350(00)00886-5.
[21] X. Li, C. Liang, Y. Guo, et al., Clinical translation of long-acting drug delivery systems for posterior capsule opacification prophylaxis, Pharmaceutics 15 (4) (2023) 1235–1259, https://doi.org/10.3390/pharmaceutics15041235.
[22] K. Park, S. Skidmore, J. Hadar, et al., Injectable, long-acting PLGA formulations: analyzing PLGA and understanding microparticle formation, J. Contr. Release 304 (2019) 125–134, https://doi.org/10.1016/j.jconrel.2019.05.003.
[23] F. Danhier, E. Ansorena, J.M. Silva, et al., PLGA-based nanoparticles: an overview of biomedical applications, J. Contr. Release 161 (2012) 505–522, https://doi.org/10.1016/j.jconrel.2012.01.043.
[24] S. Fredenberg, M. Wahlgren, M. Reslow, et al., The mechanisms of drug release in poly(lactic-co-glycolic acid)-based drug delivery systems–a review, Int. J. Pharm. 415 (2011) 34–52, https://doi.org/10.1016/j.ijpharm.2011.05.049, 20110527.
[25] J.E. Chang-Lin, M. Attar, A.A. Acheampong, et al., Pharmacokinetics and pharmacodynamics of a sustained-release dexamethasone intravitreal implant, Invest. Ophthalmol. Vis. Sci. 52 (2011) 80–86, https://doi.org/10.1167/iovs.10-5285, 20110105.
[26] P.E. Sirinek, M.M. Lin, Intracameral sustained release bimatoprost implants (Durysta), Semin. Ophthalmol. 37 (2022) 385–390, https://doi.org/10.1080/08820538.2021.1985145.
[27] G. Jiang, H. Jia, J. Qiu, et al., PLGA nanoparticle platform for trans-ocular barrier to enhance drug delivery: a comparative study based on the application of oligosaccharides in the outer membrane of carriers, Int. J. Nanomed. 15 (2020) 9373–9387, https://doi.org/10.2147/IJN.S272750, 20201124.
[28] A.K. Sah, P.K. Suresh, V.K. Verma, PLGA nanoparticles for ocular delivery of loteprednol etabonate: a corneal penetration study, Artif. Cells, Nanomed. Biotechnol. 45 (2017) 1–9, https://doi.org/10.1080/21691401.2016.1203794, 20160708.
[29] H. Gupta, M. Aqil, R.K. Khar, et al., Sparfloxacin-loaded PLGA nanoparticles for sustained ocular drug delivery, Nanomedicine 6 (2010) 324–333, https://doi.org/10.1016/j.nano.2009.10.004, 20091023.

[30] Y. Zhang, M. Huo, J. Zhou, et al., DDSolver: an add-in program for modeling and comparison of drug dissolution profiles, AAPS J. 12 (2010) 263–271, https://doi.org/10.1208/s12248-010-9185-1, 20100406.
[31] Z. Zhang, X. Wang, R. Zhu, et al., Synthesis and characterization of serial random and block-copolymers based on lactide and glycolide, Polym. Sci. B 58 (2016) 720–729, https://doi.org/10.1134/S1560090416060191.
[32] H.S. Mansur, C.M. Sadahira, A.N. Souza, et al., FTIR spectroscopy characterization of poly (vinyl alcohol) hydrogel with different hydrolysis degree and chemically crosslinked with glutaraldehyde, Mater. Sci. Eng. C 28 (2008) 539–548, https://doi.org/10.1016/j.msec.2007.10.088.
[33] Sigma-Aldrich. IR Spectrum Table & Chart https://www.sigmaaldrich.com/US/en/technical-documents/technical-article/analytical-chemistry/photometry-and-reflectometry/ir-spectrum-table (accessed October 26 2022).
[34] G. Singh, T. Kaur, R. Kaur, et al., Recent biomedical applications and patents on biodegradable polymer- PLGA, Int. J. Pharmacol. Pharmaceut. Sci. 1 (2014) 30–42.
[35] P.L. Ritger, N.A. Peppas, A simple equation for description of solute release I. Fickian and non-fickian release from non-swellable devices in the form of slabs, spheres, cylinders or discs, J. Contr. Release 5 (1987) 23–36, https://doi.org/10.1016/0168-3659(87)90034-4.
[36] O. Ivan Martinez-Munoz, C. Elizabeth Mora-Huertas, Nanoprecipitation technology to prepare carrier systems of interest in pharmaceutics: an overview of patenting, Int. J. Pharm. 614 (2022) 121440–20220105, https://doi.org/10.1016/j.ijpharm.2021.121440.
[37] M. Iqbal, N. Zafar, H. Fessi, et al., Double emulsion solvent evaporation techniques used for drug encapsulation, Int. J. Pharm. 496 (2015) 173–190, https://doi.org/10.1016/j.ijpharm.2015.10.057, 20151029.
[38] F. Ramazani, W. Chen, C.F. van Nostrum, et al., Strategies for encapsulation of small hydrophilic and amphiphilic drugs in PLGA microspheres: state-of-the-art and challenges, Int. J. Pharm. 499 (2016) 358–367, https://doi.org/10.1016/j.ijpharm.2016.01.020, 20160112.
[39] M.C. Operti, A. Bernhardt, S. Grimm, et al., PLGA-based nanomedicines manufacturing: technologies overview and challenges in industrial scale-up, Int. J. Pharm. 605 (2021), 20210616, https://doi.org/10.1016/j.ijpharm.2021.120807, 120807.
[40] S.J. Shepherd, D. Issadore, M.J. Mitchell, Microfluidic formulation of nanoparticles for biomedical applications, Biomaterials 274 (2021), 120826, https://doi.org/10.1016/j.biomaterials.2021.120826.
[41] E. Chiesa, R. Dorati, T. Modena, et al., Multivariate analysis for the optimization of microfluidics-assisted nanoprecipitation method intended for the loading of small hydrophilic drugs into PLGA nanoparticles, Int. J. Pharm. 536 (2018) 165–177, https://doi.org/10.1016/j.ijpharm.2017.11.044, 20171124.
[42] R. Karnik, F. Gu, P. Basto, et al., Microfluidic platform for controlled synthesis of polymeric nanoparticles, Nano Lett. 8 (2008) 2906–2912, https://doi.org/10.1021/nl801736q.
[43] X. Song, Y. Zhao, W. Wu, et al., PLGA nanoparticles simultaneously loaded with vincristine sulfate and verapamil hydrochloride: systematic study of particle size and drug entrapment efficiency, Int. J. Pharm. 350 (2008) 320–329, https://doi.org/10.1016/j.ijpharm.2007.08.034.
[44] A. Budhian, S.J. Siegel, K.I. Winey, Haloperidol-loaded PLGA nanoparticles: systematic study of particle size and drug content, Int. J. Pharm. 336 (2007) 367–375, https://doi.org/10.1016/j.ijpharm.2006.11.061, 20061205.
[45] D.J. Hines, D.L. Kaplan, Poly(lactic-co-glycolic) acid-controlled-release systems: experimental and modeling insights, Crit. Rev. Ther. Drug Carrier Syst. 30 (2013) 257–276, https://doi.org/10.1615/critrevtherdrugcarriersyst.2013006475.
[46] M.L. Bruschi, 5 - mathematical models of drug release, in: M.L. Bruschi (Ed.), Strategies to Modify the Drug Release from Pharmaceutical Systems, Woodhead Publishing, 2015, pp. 63–86.
[47] T. Govender, S. Stolnik, M.C. Garnett, et al., PLGA nanoparticles prepared by nanoprecipitation: drug loading and release studies of a water soluble drug, J. Contr. Release 57 (1999) 171–185, https://doi.org/10.1016/S0168-3659(98)00116-3.
[48] A. Budhian, S.J. Siegel, K.I. Winey, Controlling the in vitro release profiles for a system of haloperidol-loaded PLGA nanoparticles, Int. J. Pharm. 346 (2008) 151–159, https://doi.org/10.1016/j.ijpharm.2007.06.011, 20070616.
[49] A. Budhian, S.J. Siegel, K.I. Winey, Production of haloperidol-loaded PLGA nanoparticles for extended controlled drug release of haloperidol, J. Microencapsul. 22 (2005) 773–785, https://doi.org/10.1080/02652040500273753.
[50] X. Huang, C.S. Brazel, On the importance and mechanisms of burst release in matrix-controlled drug delivery systems, J. Contr. Release 73 (2001) 121–136, https://doi.org/10.1016/S0168-3659(01)00248-6.
[51] W. Li, J. Tang, D. Lee, et al., Clinical translation of long-acting drug delivery formulations, Nat. Rev. Mater. 7 (2022) 406–420, https://doi.org/10.1038/s41578-021-00405-w.
[52] J.J. Kang-Mieler, K.M. Rudeen, W. Liu, et al., Advances in ocular drug delivery systems, Eye 34 (2020) 1371–1379, https://doi.org/10.1038/s41433-020-0809-0, 20200218.
[53] Y. Yeo, K. Park, Control of encapsulation efficiency and initial burst in polymeric microparticle systems, Arch Pharm. Res. (Seoul) 27 (2004) 1–12, https://doi.org/10.1007/BF02980037.